ACOUSTIC CENTER AND ORIENTATION ANALYSIS OF SOUND-RADIATION RECORDED WITH A SURROUNDING SPHERICAL MICROPHONE ARRAY

Daniel Deboy, Franz Zotter

Institute of Electronic Music and Acoustics
University of Music and Performing Arts
Inffeldgasse 10/3, Graz, Austria
daniel.deboy@student.kug.ac.at, zotter@iem.at

ABSTRACT

Sound sources and musical instruments are assumed to posess an acoustic center from which sound radiates and a directivity which describes the dependency of the sound radiation on the direction. Consequently, it should be possible to assign a center and an orientation to a source by the sound it radiates. Surrounding spherical microphone arrays have been built to identify the entire sound-radiation of a source simultaneously at many directions. However, there are no established algorithms for extracting the acoustic center and orientation of sound sources from the spherical microphone arrays data. This paper considers suitable acoustic center and orientation analysis algorithms and shows some practical case studies.

1. INTRODUCTION

It is possible to obtain a complete image of all the sound radiated from a musical instrument by taking recordings with a spherical microphone-array surrounding the instrument. This image contains the most important acoustic features associated with the musical instrument. Therefore, such recordings are considered an invaluable innovation in immersive simulation of room acoustics and its perception, and above all, the closer investigation of the musical acoustics of instruments. Most interestingly, the image obtained does not only contain the sound of the instrument and its directivity pattern, but may also reveal its orientation and position, and possibly more, in principle. This contribution focuses on the analysis of sound-radiation recordings as to identify some of these seemingly secondary features. However clearly, the motivation for this particular goal is not pure curiosity, whether the localization of the acoustic center of an instrument and its orientation is feasible. Much more, our motivation is about obtaining a parametric version of sound-radiation signals that is separate from orientation and position of the musical instrument. If this separation works successfully, a great simplification of the sound-radiation signal can be expected. This is because localization allows to revert off-centered acoustical origins to the center of the spherical array and hereby minimize the required angular resolution. On the other hand, orientation tracking allows to compensate for rotational movements in the sound-radiation data, and hereby stabilizes the analysis of the directivity pattern. The following sections of the paper are divided into three parts:

Sec. 2 discusses the mathematical and physical basics. This includes an introduction into the base-functions of the spherical exterior problem, i.e. radiating sound fields, the identification of their coefficients from discrete array measurements, and a brief introduction into translation and rotation.

Sec. 3 discusses ways of rotational matching using a compact discrete set of possible rotation matrices and a correlation measure for the array observations. Experimental results using a trumpet are provided in this section.

Sec. 4 discusses ways of acoustic centering (or alignment, cp. [1]) for array observations by two kinds of cost functions that become extremal if a superior center of decomposition has been found. The two cost functions of concern include a simple interference-based measure and a robust centroid of the spherical harmonic moments. Some practical results can be given.

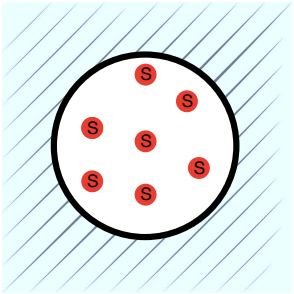

Figure 1: Illustration of the spherical exterior problem. All sound-sources are located within the microphone array, the hatchure marks the homogeneous sound-field (free of obstacles/boundaries/sources).

2. SPHERICAL EXTERIOR PROBLEM

The spherical base-solution (math./phys.) are capable of fully expanding sound fields that radiate from a radial point of origin $r = 0$ with the coefficients c_{nm}

$$p(kr, \boldsymbol{\theta}) = \sum_{n=0}^{\infty} \sum_{m=-n}^{n} \underbrace{c_{nm} h_n^{(2)}(kr)}_{:=\psi_n^m(kr)} Y_n^m(\boldsymbol{\theta}), \qquad (1)$$

the spherical Hankel-functions[1] $h_n^{(2)}(kr)$ depending on the wave-number $k = \omega/c$, ($\omega = 2\pi f$,

[1]It is a matter of convention which kind $h_n^{(1)}(kr)$, or $h_n^{(2)}(kr)$ of Hankel function to use. This paper uses the spherical Hankel function of the second kind.

$c \approx 343\mathrm{m/s}$), and the radius r, and the spherical harmonic $Y_n^m(\boldsymbol{\theta})$ depending on the cartesian unit vector $\boldsymbol{\theta} = (\cos(\varphi)\sin(\vartheta), \sin(\varphi)\sin(\vartheta), \cos(\vartheta))^{\mathrm{T}}$ the direction of which depending on azimuth φ and zenith ϑ, cf. [2, 3, 4].

As the coefficients c_{nm} fully describe the radial and angular propagation of the field, e.g. sound-pressure, they can be called the *wave-spectrum*. The term $\psi_n^m(kr) = c_{nm}\, h_n^{(2)}(kr)$ marked in eq. (1) is called *spherical wave-spectrum* as defined in [2]. It describes the sound-field, e.g. pressure, expanded into spherical harmonics at any sphere of constant radius kr and is defined by the transform integral

$$\psi_n^m(kr) = \int_{\mathbb{S}^2} p(kr, \boldsymbol{\theta}) Y_n^m(\boldsymbol{\theta}) d\boldsymbol{\theta}. \tag{2}$$

Assuming the L discrete observations of the sound-pressure by a spherical array to be a linear combination of spherical harmonics

$$\boldsymbol{p}_{\mathrm{L}} = \boldsymbol{Y}_{\mathrm{N}}\, \hat{\boldsymbol{\psi}}_{\mathrm{N}}, \tag{3}$$

$$\text{with } \boldsymbol{Y}_{\mathrm{N}} = \begin{pmatrix} Y_0^0(\boldsymbol{\theta}_1) & Y_1^{-1}(\boldsymbol{\theta}_1) & \dots & Y_{\mathrm{N}}^{\mathrm{N}}(\boldsymbol{\theta}_1) \\ Y_0^0(\boldsymbol{\theta}_2) & Y_1^{-1}(\boldsymbol{\theta}_2) & \dots & Y_{\mathrm{N}}^{\mathrm{N}}(\boldsymbol{\theta}_2) \\ \vdots & \vdots & \ddots & \vdots \\ Y_0^0(\boldsymbol{\theta}_{\mathrm{L}}) & Y_1^{-1}(\boldsymbol{\theta}_{\mathrm{L}}) & \dots & Y_{\mathrm{N}}^{\mathrm{N}}(\boldsymbol{\theta}_{\mathrm{L}}) \end{pmatrix}, \tag{4}$$

an angularly band-limited version $\psi_n^m(kr) = 0 : n > \mathrm{N}$ of the *spherical wave-spectrum* $\boldsymbol{\psi}_{\mathrm{N}}$ is obtained by matrix inversion

$$\hat{\boldsymbol{\psi}}_N(kr) = \boldsymbol{Y}_N^{-1} \boldsymbol{p}_L. \tag{5}$$

The *wave-spectrum* $\boldsymbol{c}_N$ is calculated from eq. (5) by a diagonal matrix $\boldsymbol{H}_{\mathrm{N}}$ containing the associated radial propagation terms

$$\boldsymbol{c}_N = \boldsymbol{H}_N^{-1} \hat{\boldsymbol{\psi}}_N(kr) = \boldsymbol{H}_N^{-1} \boldsymbol{Y}_N^{-1} \boldsymbol{p}_L, \tag{6}$$

$$\boldsymbol{H}_N = \mathrm{diag}_{\mathrm{N}}\{h_n^{(2)}(kr)\}. \tag{7}$$

2.1. Coordinate transforms: Re-expansion into spherical base solutions

Coordinate transform of the following types

$$\boldsymbol{r}' = \boldsymbol{r} + (0, 0, d_z)^{\mathrm{T}}, \quad \text{coaxial translation,} \tag{8}$$

$$\boldsymbol{r}' = \boldsymbol{Q}\, \boldsymbol{r}, \quad \text{rotation, } \boldsymbol{Q}\, \boldsymbol{Q}^{\mathrm{T}} = \boldsymbol{Q}^{\mathrm{T}}\, \boldsymbol{Q} = \boldsymbol{I} \tag{9}$$

express what happens if the sources inside the spherical array are displaced or being rotated. Note that arbitrary translations by a shift d can be decomposed into rotations and translations in d_z, cf. [3]. A sound-field described by the *wave-spectrum* c_{nm} at $\boldsymbol{r}$ can be re-expanded into a *wave-spectrum* c'_{nm} at $\boldsymbol{r}'$. Both types of coordinate transforms yield different mappings $c_{nm} \xrightarrow{\boldsymbol{Q},\, d_z} c'_{nm}$, cf. [3, 5, 1]

$$c'_{nm} = \sum_{n'} c_{n'm}\, T_{n'n}^m(d_z), \quad \text{coaxial translation,} \tag{10}$$

$$c'_{nm} = \sum_{m'} c_{nm'}\, T_n^{m'm}(\boldsymbol{Q}), \quad \text{rotation.} \tag{11}$$

In particular, rotation does not affect the angular band-limitation $c'_{nm} = 0 : n > \mathrm{N}$, whereas translation tends to create components of higher orders $c'_{nm} \neq 0 : n > \mathrm{N}$. That also means, that the assumption of a band-limited *spherical wave-spectrum* $\psi_n^m(kr)$ in eq. (5) may not always hold for arbitrarily shifted sources. Nevertheless, this assumption is kept to allow for the calculation of a band-limited *spherical wave-spectrum* by eq. (5), using hyperinterpolation [6, 7].

2.1.1. Band-limitation of misaligned sources

A correct representation of a source of known angular band-limit N after a displacement by d requires the re-expansion to have wave-spectral coefficients of a higher band-limit, i.e. $\mathrm{N}' > \mathrm{N}$. For the present surrounding spherical array analysis this means off-center sound sources cause higher-order components that technically need to be resolved by the array without spatial misinterpretations, i.e. aliasing [8, 7]. A rough rule-of thumb could be given as

$$\mathrm{N}' \geq \mathrm{N} + kd. \tag{12}$$

However, it is hard to know or estimate the band-limit N of an unidentified source. Even more, the misalignment d of its acoustic center from the center of the measurement array is hard to know or estimate in advance.

Therefore, as a working hypethesis, let us *assume* the correctness of the *wave-spectrum* c_{nm} calculated in eq. (6).

3. ROTATIONAL MATCHING

For tracking the angular orientation of the musical instrument between two time instants t and t', a spherical correlation measure can be optimized that compares array patterns after rotation. As the array delivers observations at discrete locations, it is more convenient to perform spherical correlations on the interpolated radiation patterns. The best rotational match is achieved by maximizing the correlation function

$$c(\boldsymbol{Q}) = \frac{\boldsymbol{\psi}_{\mathrm{N}}^{\mathrm{H}}\, \boldsymbol{T}(\boldsymbol{Q})\, \boldsymbol{\psi}'_{\mathrm{N}}}{\|\, \boldsymbol{\psi}_{\mathrm{N}}\| \|\boldsymbol{\psi}'_{\mathrm{N}}\|} \tag{13}$$

of the *spherical wave-spectra* $\boldsymbol{\psi}_{\mathrm{N}}$ and $\boldsymbol{\psi}'_{\mathrm{N}}$. The symbol $\boldsymbol{T}(\boldsymbol{Q})$ in the above measure expresses the rotation operator eq. (11).

The 3×3 rotation matrix $\boldsymbol{Q}$ are an element of the special orthogonal matrices $\mathrm{SO}(3)$, i.e. $\boldsymbol{Q}^{\mathrm{T}}\boldsymbol{Q} = \boldsymbol{Q}\, \boldsymbol{Q}^{\mathrm{T}} = \boldsymbol{I}$ and $\det\{\boldsymbol{Q}\} = +1$. Rotation matrices have three continuous degrees of freedom that can be varied in order to observe $c(\boldsymbol{Q})$, but they do not change monotonically with these angles. In order to obtain a compact but representative discrete search space for $\boldsymbol{Q}$, practical considerations on the discretization of the rotation group SO(3) follow in the next section.

3.1. Discrete set of rotations

Every rotation can be represented by three angles, the Euler-angles, e.g.

$$\boldsymbol{Q} = \boldsymbol{Q}_z(\alpha)\, \boldsymbol{Q}_y(\beta)\, \boldsymbol{Q}_z(\gamma), \tag{14}$$

$$\text{with } \boldsymbol{Q}_z(\angle) = \begin{pmatrix} \cos(\angle) & \sin(\angle) & 0 \\ -\sin(\angle) & \cos(\angle) & 0 \\ 0 & 0 & 1 \end{pmatrix},$$

$$\text{and } \boldsymbol{Q}_y(\beta) = \begin{pmatrix} \cos(\beta) & 0 & \sin(\beta) \\ 0 & 1 & 0 \\ -\sin(\beta) & 0 & \cos(\beta) \end{pmatrix}.$$

In order to find a well-separated and uniform set of rotations $\{\boldsymbol{Q}_q\}_{q=1\dots\mathrm{Q}}$, a distance measure of two rotation matrices $\boldsymbol{Q}_1$ and $\boldsymbol{Q}_2$ can be defined according to [9]

$$\gamma_{dist} = \arccos\big(\frac{1}{2}(\boldsymbol{T}r(\boldsymbol{Q}_1\boldsymbol{Q}_2^{\mathrm{T}}) - 1\big). \tag{15}$$

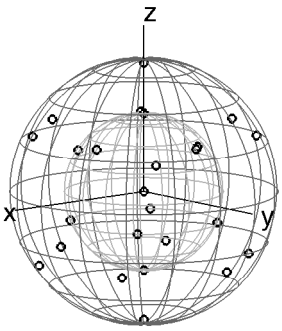

Figure 2: Example rotational test set: three spherical radii represent rotations by $\gamma = \{0, \frac{\pi}{2}, \pi\}$; corresponding layers are sampled by an increasing number of nodes representing discrete directions of rotation axes.

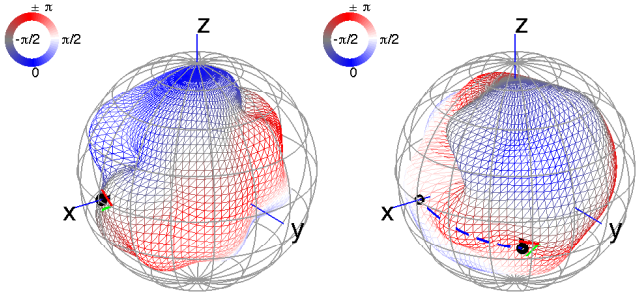

(b) t=0 sec (c) t=5 sec

Figure 3: Rotational tracking of the radiation patterns of a moving trumpet. The dashed line shows the tracked trace interpolated between two sample blocks.

This metric could be a starting point for searching well-separated sets with optimization.

Another, more convenient way is proposed here, that is mostly uniform and well-separated. The rotation angles α, β, γ can be expressed as a unit vector in $\mathbb{R}^4$, i.e. as points on the unit-hypersphere $\mathbb{S}^3$

$$\boldsymbol{q} = \begin{pmatrix} \cos(\gamma/2) \\ \sin(\gamma/2)\sin(\beta) \\ \sin(\gamma/2)\cos(\beta)\sin(\alpha) \\ \sin(\gamma/2)\cos(\beta)\cos(\alpha) \end{pmatrix}. \tag{16}$$

The software tool [10] from Paul Leopardi [11] allows to find uniformly distributed nodes on $\mathbb{S}^3$. Note that the southern hyper-hemisphere is not used as corresponding rotations $\boldsymbol{Q}$ can be expressed in the domain $0 \leq \gamma \leq 180°$. Moreover, the hereby found discrete search space can be limited to smaller rotation angles if the considered time-steps do not allow for great movements. Fig. 2 gives an example of a discrete set of rotations depicting the discrete points in the mapping of $\mathbb{S}^3$ on $\mathbb{R}^3$

$$\boldsymbol{q}^{(3)} = \begin{pmatrix} 0 & 1 & 0 & 0 \\ 0 & 0 & 1 & 0 \\ 0 & 0 & 0 & 1 \end{pmatrix} \boldsymbol{q}. \tag{17}$$

3.2. Case study using a trumpet

Fig. 3 shows an example of rotational tracking of a trumpet in the IEM array [6]; its pick-up positions lie at $r = 1.2$m. The *spherical wave-spectra* determined by the absolute sound-pressures $\hat{\boldsymbol{\psi}}_\mathrm{N} = \boldsymbol{Y}_\mathrm{N}^{-1} |\boldsymbol{p}|$ seem to be more robust for rotational tracking, however might become ambiguous for single spherical harmonics as radiation patterns. In the first time-frame shown in the figure the instrument is assumed to be the reference direction x. In the second time-frame, this direction has obviously changed.

4. ACOUSTIC CENTERING / POSITION TRACKING

Unlike rotational matching, acoustic centering does not require comparison of two different spherical patterns. Despite the proposed acoustic centering (or alignment [1]) method is only referring to the shifted $\boldsymbol{\psi}'_\mathrm{N}$ and neglects possible errors in the interpolation of discrete spherical patterns, it is shown to produce convincing results for position tracking; even for regarding single frequencies only.

4.1. Cost functions for centering

Two approaches have been examined for the static tracking of the acoustic center. One is the complex-squared sum of the discrete sound pressure distribution

$$\begin{aligned} J_{ssc}(\boldsymbol{d}) &= 1 - \left| \frac{\int p(\boldsymbol{\theta})^2 \, d\boldsymbol{\theta}}{\int |p(\boldsymbol{\theta})|^2 \, d\boldsymbol{\theta}} \right| \\ &= 1 - \left| \frac{\boldsymbol{\psi'}_{\mathrm{N}'}^{\mathrm{T}} \, \boldsymbol{\psi}'_{\mathrm{N}'}}{\|\boldsymbol{\psi}'_{\mathrm{N}'}\|^2} \right|, \end{aligned} \tag{18}$$

for real-valued spherical harmonics. The shifted *spherical wave-spectrum* $\boldsymbol{\psi}'_{\mathrm{N}'} = \boldsymbol{H}\,\boldsymbol{T}(\boldsymbol{d})\,\boldsymbol{H}^{-1}\,\boldsymbol{\psi}_\mathrm{N}$ is found by eq. (10). The other cost function regards the center of mass of the spherical harmonics components

$$J_{mc}(\boldsymbol{d}) = \frac{\boldsymbol{c'}_{\mathrm{N}'}^{H} \mathrm{diag}_{\mathrm{N}'}\{w_n\} \boldsymbol{c'}_{\mathrm{N}'}}{\boldsymbol{c'}_{\mathrm{N}'}^{H} \boldsymbol{c'}_{\mathrm{N}'}}, \tag{19}$$

where w_n can be any penalizing weight increasing with the order n, e.g. $n + 1$. Both cost functions can be evaluated within the volume of the array. Fig. 4 shows an example of a simulated omni-directional source located at the center of the array, the cost functions are evaluated along the z-axis of the array. A global minimum should give the estimated dislocation of the acoustic center of the sound source. Obviously, J_{mc} gives a less sharp but more reliable result. In [12] J_{ssc} has been shown to fail with arbitrary complex wave-spectra c_{nm}. Therefore the subsequent algorithm preferably uses J_{mc}.

4.2. Solution by optimization

Several volume sampling methods have been tested to find a global minimum of J_{mc} within a certain radial bound. The re-expansion is calculated for every sampling node. The cubic close sphere packing method has proven to be an efficient solution since several nodes have the same angular positions and others share the same radius. However, the more sophisticated non-linear optimization algorithm using the simplex-search method outperforms these simple search methods (e.g. fminsearch in

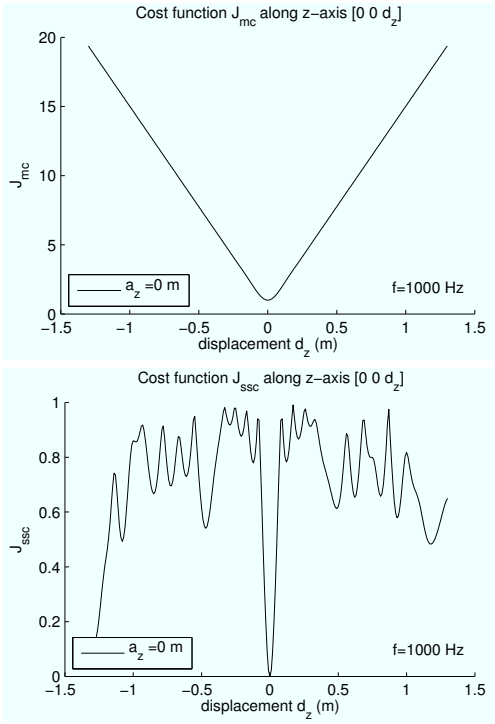

Figure 4: Cost functions evaluated along the z-axis for both suggested criteria, the complex squared sum J_{ssc} and the centroid of the wave spectra J_{mc}. An omni-directional sound-source is simulated at the origin of the array.

MATLAB). The non-linear optimizer is given access to evaluation of the cost-function and autonomously optimizes for the best parameter $\boldsymbol{d}$.

Fig. 5 gives a brief estimation of the errors for the simulated monopole source inside a simulated 64-channel array, i.e. a noise-less and acoustically ideal case. The frequency after which the algorithm fails can be predicted with eq. (12). Errors at small shifts are probably due to numerical errors in the algorithm.

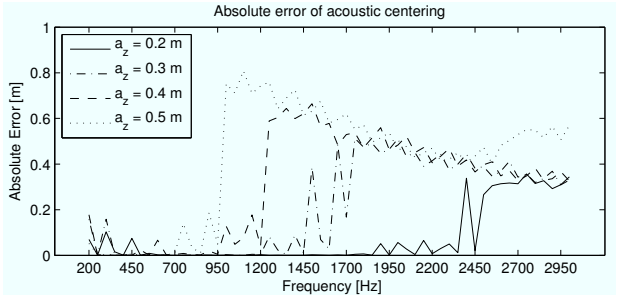

Figure 5: Analytic simulation of the absolute errors of the acoustic centering algorithm using J_{mc} with the simplex search method. Different dislocations a_z are evaluated.

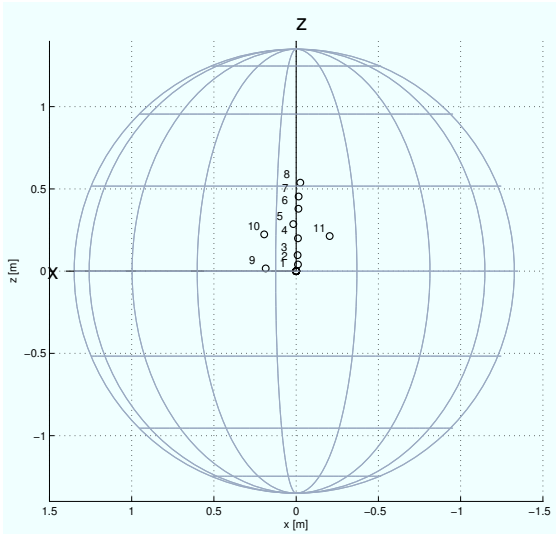

Figure 6: Experimental evaluation of the acoustic centering algorithm using J_{mc} and simplex search method. A loudspeaker in a small enclosure has been placed at different locations.

$Position$	$\boldsymbol{a}([a_x\, a_y\, a_z]\, cm)$	$-d_{min}([d_x\, d_y\, d_z]\, cm)$	$v_{error}(cm)$
1	$[0\ \ 0\ \ 0]$	$[0\ \ 0\ \ 0]$	$N.A.$
2	$[0\ \ 0\ \ 5]$	$[1\ \ 0\ \ 4]$	1.41
3	$[0\ \ 0\ \ 10]$	$[1\ \ 1\ \ 10]$	1.41
4	$[0\ \ 0\ \ 20]$	$[1\ \ 0\ \ 20]$	1
5	$[0\ \ 0\ \ 30]$	$[2\ \ 2\ \ 29]$	3
6	$[0\ \ 0\ \ 40]$	$[1\ \ 0\ \ 38]$	2.23
7	$[0\ \ 0\ \ 50]$	$[1\ \ 0\ \ 45]$	5.01
8	$[0\ \ 0\ \ 60]$	$[2\ \ 1\ \ 54]$	6.4
9	$[20\ \ 0\ \ 0]$	$[18\ \ 1\ \ 0]$	2.23
10	$[20\ \ 0\ \ 20]$	$[19\ \ 1\ \ 22]$	2.45
11	$[-20\ \ 0\ \ 20]$	$[-20\ \ 2\ \ 21]$	2.23

Table 1: Positions of the loudspeaker

Table 2: Positions of the loudspeaker, the determined localization vector criterion and the absolute error.

4.3. Case study1: Loudspeaker

To get an idea of the reliability in real-world cases, we have evaluated impulse responses of a loudspeaker in a small enclosure which is assumed to have an omni-directional radiation below a certain frequency. Measurements have been done at different positions using the exponential sweep method, the resulting impulse responses are not cut.

Fig. 6 shows the acoustic centers found by the optimization algorithm. Tab. 2 lists the test positions $\boldsymbol{a}$ of the loudspeaker and the optimization results $\boldsymbol{d}_{min}$. The relative offsets of the test positions are known and their absolute position is calibrated to position no. 1. This position has been set up closest to the origin of the array. Tab. 2 gives the absolute error of the optimization result including positioning errors of the speaker placement.

Within a radial bound of about $r = 40-50\ cm$ the algorithm gives excellent results. Outside this radial bound the results are distorted by spatial aliasing.

4.4. Case study2: Bassflute

Fig. 7 shows a centering map of a bassflute recording in the IEM array. A centering map depicts the cost functions evaluated at a slice through the spherical volume that goes through

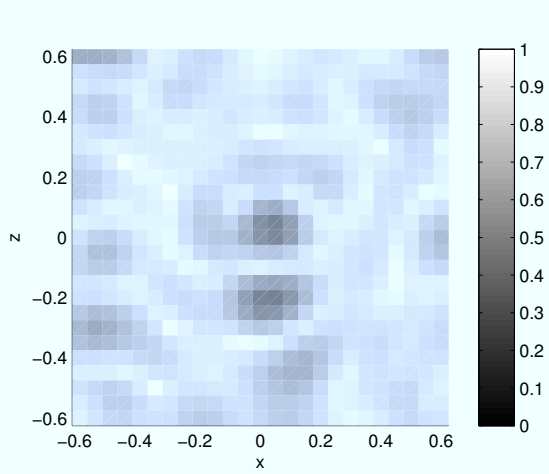

(a) 2nd partial at 526 Hz, J_{ssc} criterion

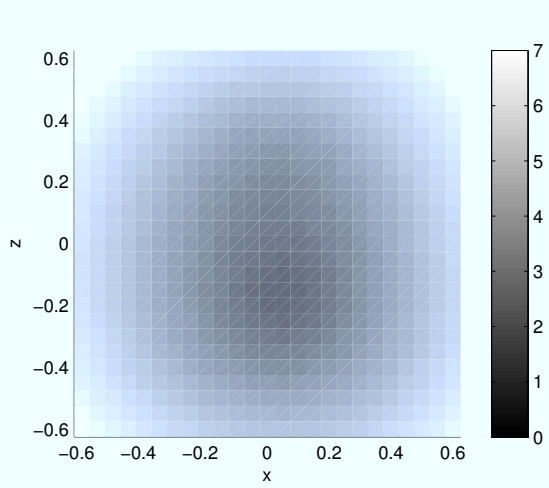

(a) 2nd partial at 526 Hz, J_{mc} criterion

Figure 7: Example of centering maps for a Bassflute recording. The spherical volume is sliced at the optimization result of the J_{mc} criterion. Both maps show the x-z-plane of the volume.

the detected acoustic center. The two effective points of radiation of the bassflute are represented as local centers revealed by the complex squared-sum criterion whereas the mass centroid criterion stays convex through the whole array volume and can therefore be used to determine a global minimum using the nonlinear optimizer.

5. CONCLUSIONS

This paper considers sound-radiation analysis with spherical arrays in order to determine the orientation and acoustic center of a sound source at a given frequency.

We presented an efficient algorithm for orientation tracking with rotational matching by spherical correlation on a suitable rotational search-space. We also gave two cost functions for detecting the acoustic center of a sound source by using the "multipole"-translation operators. For the latter algorithm, nonlinear optimization has been found superior to a discrete search

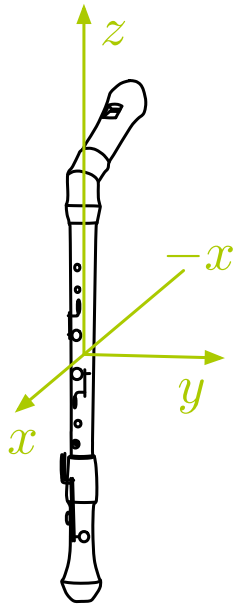

Figure 8: Orientation of the Bassflute in the IEM array [6].

space as one of the proposed cost functions is nearly convex for most scenarios.

Both algorithms have been applied to real-world data captured by the IEM spherical microphone array and seem to work convincingly. Nevertheless there are errors and limitations that have been simulated briefly.

A comprehensive study on the constellation of acoustic centers of musical instruments is subject to future research, and the errors and limits should be examined more closely.

6. REFERENCES

[1] B. Rafaely, "Spatial alignment of acoustic sources based on spherical harmonics radiation analysis," 2010.

[2] E. G. Williams, *Fourier Acoustics - Sound Radiation and Nearfield Acoustical Holography*. Academic Press, 1999.

[3] N. A. Gumerov and R. Duraiswami, *Fast Multipole Methods for the Helmholtz Equation in Three Dimensions*, 1st ed. Elsevier, 2004, no. 0-08-044371-0.

[4] F. Zotter, "Analysis and Synthesis of Sound-Radiation with Spherical Arrays," Ph.D. dissertation, Insitute of Electronic Music and Acoustics, University of Music and Performing Arts Graz, Austria, 2009.

[5] W. C. Chew, "Recurrence relations for three-dimensional scalar addition theorem," *Journal of Electromagnetic Waves and Applications*, vol. 6, no. 2, 1992.

[6] F. Hohl, "Kugelmikrofonarray zur Abstrahlungsvermessung von Musikinstrumenten," Master's thesis, Institut für Elektronische Musik und Akustik, Universität für Musik und darstellende Kunst, Graz, Österreich, November 2009.

[7] F. Zotter, "Sampling strategies for acoustic holography/ holophony on the sphere," in *NAG-DAGA, Rotterdam*, 2009.

[8] B. Rafaely, B. Weiss, and E. Bachmat, "Spatial aliasing in spherical microphone arrays," *IEEE Transactions on Signal Processing*, vol. 55, March 2007.

[9] J. C. Mitchell, "Discrete uniform sampling of rotation groups using orthogonal images," *Departments of Mathematics and Biochemistry*, 2007.

[10] P. Leopardi. (2010) Equal area partitioning toolbox for MATLAB. [Online]. Available: http://eqsp.sourceforge.net/

[11] ——, "Distributing points on the sphere: Partitions, separation, quadrature and energy," Ph.D. dissertation, School of Mathematics and Statistics, Departement of Applied Mathematics, University of New South Wales, November 2006.

[12] D. Deboy, "Acoustic centering and rotational tracking in surrounding spherical microphone arrays," 2010.